Published in final edited form as:
Nat Neurosci. 2008 September ; 11(9): 1024–1034. doi:10.1038/nn.2172.

Age-dependent epigenetic control of differentiation inhibitors is critical for remyelination efficiency

Siming Shen[1,5], **Juan Sandoval**[1,5], **Victoria A Swiss**[1], **Jiadong Li**[1], **Jeff Dupree**[2], **Robin J M Franklin**[3], and **Patrizia Casaccia-Bonnefil**[1,4]

1*Department of Neuroscience and Cell Biology, Robert Wood Johnson Medical School, 675 Hoes Lane, Piscataway, New Jersey 08854, USA.*

2*Department of Anatomy and Neurobiology, Virginia Commonwealth University Medical Campus, Box 980709, Richmond, Virginia 23298, USA.*

3*Cambridge Centre for Brain Repair and Department of Veterinary Medicine, University of Cambridge, Madingley Road, Cambridge CB3 0ES, UK.*

Abstract

The efficiency of remyelination decreases with age, but the molecular mechanisms responsible for this decline remain only partially understood. In this study, we show that remyelination is regulated by age-dependent epigenetic control of gene expression. In demyelinated young brains, new myelin synthesis is preceded by downregulation of oligodendrocyte differentiation inhibitors and neural stem cell markers, and this is associated with recruitment of histone deacetylases (HDACs) to promoter regions. In demyelinated old brains, HDAC recruitment is inefficient, and this allows the accumulation of transcriptional inhibitors and prevents the subsequent surge in myelin gene expression. Defective remyelination can be recapitulated *in vivo* in mice receiving systemic administration of pharmacological HDAC inhibitors during cuprizone treatment and is consistent with *in vitro* results showing defective differentiation of oligodendrocyte progenitors after silencing specific HDAC isoforms. Thus, we suggest that inefficient epigenetic modulation of the oligodendrocyte differentiation program contributes to the age-dependent decline in remyelination efficiency.

Remyelination is the regenerative process in which new myelin sheaths are restored to demyelinated axons. In the CNS, this process is mediated by the recruitment and differentiation of a widespread population of adult stem and progenitor cells, called oligodendrocyte progenitor cells (OPCs), into myelin sheath–forming oligodendrocytes[1–3]. Remyelination can be a highly efficient process resulting in complete healing in both experimental models and clinical demyelinating diseases, including multiple sclerosis[4–8]. However, for reasons that are not fully understood, remyelination may be incomplete or fail in multiple sclerosis, leaving axons demyelinated and vulnerable to atrophy[9]. For this reason, therapeutic promotion of

Correspondence should be addressed to P.C.-B. (patrizia.casaccia@mssm.edu).
[4]Present address: Department of Neuroscience and Genetics and Genomics, Mount Sinai School of Medicine, One Gustave Levy Place Box 1065, New York, New York 10029, USA.
[5]These authors contributed equally to this work.

AUTHOR CONTRIBUTIONS

S.S. and J.S. performed the majority of the experiments and data analysis. J.L. contributed to the *in vivo* experiments and V.A.S. to the silencing experiments. J.D. performed the ultrastructural analysis. R.J.M.F. contributed to the initial phase of the project and helped with text writing and editing. P.C.-B. was responsible for planning the experiments, supervising the project, critically analyzing the results and writing the manuscript.

Published online at http://www.nature.com/natureneuroscience/

remyelination represents an attractive option for preventing the axonal loss that underlies the progressive deterioration frequently associated with the later stages of the disease[10,11].

One of the most profound factors affecting remyelination is aging: as with other regenerative processes, remyelination becomes less efficient with age[12], an effect that ismore pronounced inmales than in females[13]. This age-associated effect is due to impairment of OPC recruitment and differentiation[14], of which inefficient differentiation is the more significant, as increasing the availability of OPCs during remyelination in old animals does not enhance remyelination efficiency[15]. Inefficient OPC differentiation in aging mirrors non-remyelinating plaques in humans with multiple sclerosis, which are replete with oligodendrocyte-lineage cells that fail to differentiate into remyelinating oligodendrocytes[16–18]. Thus, understanding OPC differentiation is central to explaining remyelination failure and the age-associated decline in remyelination, and hence identifying potential therapeutic targets.

Environmental changes associated with aging and remyelination include modifications of the innate immune and growth factors responses to demyelination[19,20]. However, adding single growth factors to old animals does not increase remyelination efficiency, suggesting the existence of multiple regulators of remyelination[21]. Conversely, transcriptional regulators of remyelination such as Olig1 profoundly affect remyelination efficiency[22], acting with other transcription factors to modulate myelin gene expression[23]. Environmental effects on gene expression are modulated by changes in the epigenome that include post-translational modifications of nucleosomal histones[24–26]. Preventing histone deacetylation is detrimental for developmental myelination[27], although it is unknown whether similar mechanisms affect OPC differentiation during remyelination.

Here we use a toxin-induced mouse model of demyelination and remyelination[28] to test the hypotheses that (i) remyelination efficiency requires deacetylation of nucleosomal histones, which leads to the execution of a complex transcriptional program of OPC differentiation, and (ii) this process is altered during aging.

RESULTS

Transcriptional response in remyelinating young mice

To test the hypothesis that remyelination involves epigenetic modulation of gene expression, we first used the cuprizone model of demyelination in young (8-week-old) C57BL/6 mice. Mice fed a cuprizone-containing diet for 6 weeks developed demyelination of the dorsal corpus callosum, followed by spontaneous remyelination on removal of cuprizone (6–8 weeks) (data not shown). Decreased myelin gene transcripts were detected in the corpus callosum of cuprizone-fed mice after 2 weeks of cuprizone treatment (Fig. 1a). The expression remained low until 4 weeks of treatment and then spontaneously increased until 6 weeks (Fig. 1a). The decline in transcripts was paralleled by decreased myelin proteins evident at 4 weeks and persisting until 6 weeks (Fig. 1b). The early decrease in myelin gene transcripts was associated with an increase in *Sox2*, a marker of neural stem cells[26,29], likely indicating the mobilization of cells mediating remyelination (Fig. 1c). The transcriptional response associated with repair was further characterized by the subsequent decrease of *Sox2* and other transcriptional inhibitors (*Hes1, Hes5, Id2* and *Id4*) after 4 weeks of cuprizone (Fig. 1d). The temporal downregulation of inhibitors at 4 weeks was followed by increased transcripts of myelin genes and *Olig1*, a transcription factor critical for remyelination at 6 weeks (Fig. 1c). These data indicate a dynamically regulated transcriptional network during remyelination.

We hypothesized that this coordinated regulation is orchestrated by the activity of chromatin-modifying enzymes required for developmental myelination[27]. Densitometric quantification of western blots (Fig. 1e) and quantitative reverse transcription (qRT)-PCR (Supplementary

Fig. 1 online) showed a statistically significant increase of class I HDAC isoforms after 4 weeks of cuprizone, followed by return to control levels at 6 weeks. The HDAC1 isoform showed the greatest increase by western blot analysis (Fig. 1e). HDAC1 was predominantly detected in the nuclei of PDGFRα$^+$ OPCs and to some extent also in GFAP$^+$ astrocytes but not in Mac1$^+$ inflammatory cells in the corpus callosum of cuprizone-treated mice (Fig. 1f). Because class I nuclear HDACs have been associated with transcriptional repression, we asked whether the pattern of expression of Sox2, a transcription factor associated with the maintenance of multipotency, and Hes5, an inhibitor of OPC differentiation, was associated with the recruitment of distinct HDAC isoforms to their promoter regions. We isolated chromatin samples from the corpus callosum of mice either untreated or treated with cuprizone for 2, 4 and 6 weeks followed by two weeks of normal diet. Immunoprecipitation was carried out with antibodies for each class I HDAC isoform, and their occupancy of the *Sox2* or *Hes5* promoter was evaluated by semiquantitative (Fig. 1g) and quantitative chromatin immunoprecipitation (qChIP) (Fig. 1h). Consistent with the changing levels of *Sox2* and *Hes5* transcripts, the levels of HDAC1 binding to their promoters were low at two weeks and high at 4 weeks (Fig. 1g).

HDAC removes acetyl groups from the tail lysine residues of histone H3. We therefore asked whether the time course of acetyl-histone H3 (AcH3) in cells of cuprizone-treated mice correlated with the pattern of HDAC expression. Immunohistochemistry using antibodies to AcH3 showed increased acetylation during the first 2 weeks of cuprizone, followed by a decrease at 4 and 6 weeks (Supplementary Fig. 2 online). To further define the cellular identity of the AcH3$^+$ cells at 2 weeks, we used antibodies for PDGFRα to label OPCs, for CD68 to label macrophages, for GFAP to label astrocytes and for Mac1 to label microglia (Fig. 2a). The majority of the AcH3$^+$ cells in the corpus callosum were PDGFRα$^+$ (66.2% ± 2.3%), the remainder being GFAP$^+$(24.4% ± 3.3%), Mac1$^+$ (9.7% ± 0.9%) or CD68$^+$ (6.3% ± 2.4%). Because histone acetylation favors the reversion of OPCs to a multipotential state[24,26], we asked whether increased Sox2 protein could also be detected in AcH3$^+$ OPCs. Double immunohistochemistry using antibodies specific for AcH3 and either Sox2 or PDGFRα showed a similar distribution and percentage of AcH3$^+$Sox2$^+$ (48.3% ± 2.4%) and AcH3$^+$PDGFRα$^+$ cells (44.6%± 4.1%) relative to the total number of AcH3$^+$ cells. Furthermore, we observed that the percentage of AcH3$^+$Sox2$^+$ cells relative to the total DAPI$^+$ population increased from 2.8% ± 1.75% in untreated controls to 48.3% ± 2.4% at 2 weeks and decreased to 9.7% ± 1.5% after 4 weeks of cuprizone treatment (Fig. 2b). Similarly, the AcH3$^+$PDGFRα$^+$ population increased from 15.7% ± 2.7% in untreated controls to 44.6% ± 4.1% at 2 weeks and then decreased to 14.6% ± 3.3% by the end of the fourth week (Fig. 2b). Together, these data suggest that HDAC activity plays a role in CNS remyelination.

Differentiation inhibitors are regulated by histone H3 acetylation

To further define the functional relationship between histone acetylation, expression of *Sox2* and *Hes5*, and remyelination, we administered the HDAC inhibitor valproic acid (VPA) during cuprizone treatment (Fig. 2c). The effect of VPA treatment on global histone acetylation was confirmed by increased AcH3 immunoreactivity in the corpus callosum of treated mice compared to saline-injected controls (data not shown). qRT-PCR of samples from VPA-treated mice showed lower levels of *Olig1* and *Mag* and higher levels of *Hes5* and *Sox2* compared to controls in the remyelinating corpus callosum (Fig. 2d). To address whether VPA treatment differentially affected the levels of *Sox2* and *Hes5* in distinct cell types, we repeated the experiment *in vitro* and tested the effect of cuprizone treatment alone or in combination with VPA in cultured OPCs, astrocytes and microglial cells. qRT-PCR analysis of samples collected from untreated and treated cells showed a VPA-induced decrease of *Olig1* and *Mag* and upregulation of *Sox2* and *Hes5* in differentiating OPC but not in proliferating OPCs, astrocytes or microglial cells (Fig. 2e). These results suggest that the VPA effect *in vivo* was mainly mediated by pharmacological inhibition of OPC differentiation.

To establish whether increased *Sox2* transcripts in response to VPA treatment resulted in increased protein levels in specific cell types, we performed immunohistochemistry (Fig. 3a). In cuprizone-treated mice, $Sox2^{+}PDFGR\alpha^{+}$ cells were detected mainly in the lateral corpus callosum and the subventricular zone. VPA treatment resulted in 1.9-fold increase of nuclear Sox2 amounts as determined by the average fluorescence intensity (Fig. 3b). To define the relationship between increased levels of acetylation and *Sox2* and *Hes5* transcripts, we performed chromatin immunoprecipitation (ChIP) with antibodies for AcH3 and, to identify promoter occupancy, for active RNA Polymerase (Pol) II (Fig. 3c,d). Samples isolated from VPA-treated mice were compared with those from saline-treated controls. Consistent with the low levels of *Sox2* and *Hes5* detected in untreated mice, low levels of RNA Pol II binding and AcH3 were detected in the regions of chromatin surrounding the *Sox2* and *Hes5* promoter in brains of saline-injected mice (Fig. 3c). qChIP showed a statistically significant increase AcH3 and RNA Pol II within the promoters of *Sox2* and *Hes5* in VPA-treated mice compared to the saline-injected controls (Fig. 3d). To determine whether the aberrant transcriptional profile induced by VPA treatment impaired remyelination, we examined the differentiation of OPCs in the corpus callosum of saline or VPA-treated mice. Immunohistochemical analysis with antibodies for PDGFRα to identify OPCs and for CC1 to identify mature oligodendrocytes showed an increase in the percentage of immature cells and decrease of mature oligodendrocytes in VPA-treated mice compared to saline-injected controls (Fig. 3e), indicating impaired OPC differentiation in the VPA-treated group.

The inefficient differentiation of OPC consequent to increased histone acetylation was associated with fewer myelinated fibers detected in the corpus callosum (Fig. 4a,b). Decreased remyelination efficiency was not associated with an aberrant pattern of immunoreactivity for $CD68^{+}$ or $Mac1^{+}$ (Supplementary Fig. 3a–d online). qRT-PCR of RNA from the corpus callosum ofmice treated with cuprizone and either saline or VPA or from cultured microglial cells showed no difference in gene expression between untreated and treated groups (Supplementary Fig. 3b,c). Similarly, no difference was detected in $GFAP^{+}$ cells between VPA-treated mice and controls (Supplementary Fig. 3d,e). To determine whether VPA treatment induced damage to callosal axons, we counted the number of $SMI\text{-}32^{+}$ axonal spheroids (Fig. 4c) in the corresponding regions of the corpus callosum in saline and VPA treated mice. A similar number was detected in the two groups (Fig. 4d), confirming that the effect of VPA on remyelination was independent of axonal pathology. These results were validated by ultrastructural analysis (Fig. 4e). Although both saline and VPA-treated mice showed a high number of small-caliber unmyelinated axons at the time of analysis (6 weeks of cuprizone diet followed by 2 weeks recovery), the percentage of large-caliber myelinated axons in the saline-treated control group ($48.1 \pm 3.8\%$, $n = 6$) was much greater than in the VPA-treated mice ($22.2 \pm 6.7\%$, $n = 6$; Fig. 4f). These results indicate that the negative effect of pharmacological HDAC inhibitors on remyelination is likely due to impaired OPC differentiation.

Inefficient epigenetic regulation in old mice

Decreased remyelination efficiency and impaired OPC differentiation are characteristic of the aging process, which is also characterized by progressive loss of epigenetic memory in mature oligodendrocytes[14,15,30]. We hypothesized that aberrant epigenetic regulation of differentiation inhibitors in OPCs could account for the age-associated impairment of spontaneous repair. To test this hypothesis, we subjected 10-month-old mice to cuprizone-induced demyelination[31]. At several time points of cuprizone treatment, we measured transcript levels of *Cnp, Mag* and *Olig1* in young and oldmice (Fig. 5a). A similar decrease in myelin gene expression was detected in young mice treated with 0.2% cuprizone and in old mice treated with 0.4% cuprizone for 4 weeks, suggesting a similar susceptibility to demyelination. The main difference between the two groups occurred during the spontaneous

remyelination phase: whereas young mice showed increased *Cnp, Mag* and *Olig1*, these were not observed in old mice (Fig. 5a). Immunohistochemical analysis at 6 weeks showed decreased immunoreactivity for myelin proteins in old mice (Supplementary Fig. 4 online). The decreased remyelination efficiency in old mice was confirmed ultrastructurally by the presence of many unmyelinated axons of a diameter above the threshold for myelination[32] (Fig. 5b). Given the similarities between cuprizone lesions in old mice and VPA-treated young mice, we hypothesized that inefficient remyelination in old mice may be due to aberrant regulation of gene expression. We counted the numbers of cells that were double-positive for HDACs 1, 2, 3 or 8 and for the OPC marker PDGFRα in the corpus callosum of old mice and found a significant decrease in $HDAC1^{+}PDGFR\alpha^{+}$ and $HDAC8^{+}PDGFR\alpha^{+}$ cells compared to the numbers in young mice (Fig. 5c). These data were consistent with the lower levels of *Hdac* transcripts detected in cuprizone-treated old mice compared to young mice (Supplementary Fig. 5 online). Because HDAC1 and HDAC8 occupy the *Sox2* promoter during remyelination in young mice (Fig. 1g,h), we asked whether the decrease of these HDAC isoforms in old mice resulted in increased Sox2 in $PDGFR\alpha^{+}$ cells (Fig. 5d). Confocal images showed increased Sox2 fluorescence intensity in the nuclei of $PDGFR\alpha^{+}$ cells in old cuprizone-treated mice during remyelination compared to that in young mice (Fig. 5d).

In agreement with previous reports[33], we observed a lower degree of microglial and macrophage infiltration in the corpus callosum of old mice compared to young ones (Fig. 6a). Quantification of microglial gene transcripts in the two age groups showed a similar pattern of activation in response to cuprizone (Fig. 6b). Immunohistochemical analysis of $GFAP^{+}$ cells (Fig. 6c) and qRT-PCR revealed a similar trend for the astrocytic cell population (Fig. 6d). Together, these data suggest that the impaired remyelination in old mice is unlikely to be a consequence of axonal damage or altered microglial or astrocytic gene expression.

A potential explanation for reduced remyelination in old mice was the occurrence of axonal damage, owing to the higher dose of cuprizone used[31]. To address this question, we treated young mice either with 0.2%cuprizone or with 0.4% cuprizone and measured the number of $SMI\text{-}32^{+}$ axonal spheroids (Fig. 7a,b). A statistically significant difference in axonal damage was detected only when the number of axonal spheroids in the medial corpus callosum of young mice on 0.2% cuprizone diet was compared with the number in old mice on a 0.4% cuprizone diet, and this is consistent with previous reports[31]. However, no difference was observed when the number of axonal spheroids in the medial corpus callosum of young mice on 0.4% cuprizone diet was compared with the number in old mice treated with the same 0.4% cuprizone dosage (Fig. 7b). We then asked whether the differences in transcriptional response associated with remyelination and the epigenetic changes could still be detected between young and old mice receiving the same dose of cuprizone treatment. qRT-PCR was performed in samples isolated from young mice treated with 0.2% and 0.4% and the results compared with those obtained from samples isolated from old mice treated with 0.4% (Fig. 7c). In agreement with an age-dependent rather than dose-dependent effect of cuprizone, a similar downregulation of *Sox2, Hes5, Id2* and *Id4* was detected in young adults treated with 0.2% or 0.4% cuprizone but not in old mice (Fig. 7c). Binding of RNA Pol II and AcH3 to the promoter region of *Sox2* and *Hes5* detected by ChIP decreased in young mice after 2 weeks, during which time remyelination commences but persisted throughout the duration of cuprizone treatment in old mice (Supplementary Fig. 6 online). Together, these data indicate that the temporal dynamics of the coordinated transcriptional response characteristic of remyelination in young but not in old mice is an age-dependent event that is not affected by the dosage of cuprizone or by the degree of axonal damage.

We then asked whether the recruitment of HDAC to the promoter regions of markers of repair was also age dependent. We performed a ChIP assay on chromatin samples isolated from the corpus callosum of young and old mice treated with 0.4% cuprizone (Fig. 7d). We used

antibodies specific for the distinct HDAC isoforms and primers for multiple regions of the *Sox2* and *Hes5* promoters (Fig. 7d–g). The pattern of recruitment of HDAC1, HDAC2 and HDAC8 to the proximal region of the *Sox2* promoter (Fig. 7d,e) and of HDAC1 and HDAC2 to the *Hes5* promoter (Fig. 7f,g) in young mice was consistent with the pattern of histone acetylation within the promoters (Supplementary Fig. 6). This pattern was also consistent with the decrease in *Sox2* and *Hes5* transcripts detected during remyelination in young mice. The recruitment of multiple HDAC isoforms to the chromatin region of *Sox2* and *Hes5* promoters detected in young mice was not observed in old mice regardless of the cuprizone dose. Together, these results further validate the existence of age-dependent differences in epigenetic regulation of gene expression during remyelination.

Finally, we asked whether the recruitment of specific HDAC isoforms to chromatin in OPCs is causally linked to their differentiation. To address this, we performed qChIP *in vitro* on immunoselected primary OPCs either maintained undifferentiated or allowed to differentiate (Fig. 8a). Consistent with the *in vivo* data, we detected increased HDAC1 and HDAC2 binding to the *Sox2* promoter in chromatin samples isolated from differentiating cells compared to undifferentiated OPCs. These data suggested that HDAC1 andHDAC2 were the primary isoforms responsible for the downregulation of Sox2 in OPCs. To further characterize the relevance of each class I HDAC isoform on the regulation of Sox2, we performed a silencing experiment in primary OPCs and assessed Sox2 in these cells after differentiation (Fig. 8b). Sox2 was downregulated in differentiating OPCs transfected with control short interfering RNAs (siRNAs) and in cells with silenced HDAC3 and HDAC8. Consistent with the ChIP data, only progenitors with efficient silencing of HDAC1 or HDAC2 showed very high Sox2 levels (Fig. 8b). These data support a necessary role of HDAC1 and HDAC2 in the downregulation of *Sox2*. To further define the relative importance of each class I HDAC isoform to oligodendrocyte differentiation, we repeated the silencing experiment and assessed differentiation based on antigenic and morphological criteria (Fig. 8c). OPCs were transfected with siRNA specific for each HDAC isoform or with control siRNA constructs. Differentiation was assessed by the loss of A2B5 immunoreactivity (amarker for early, undifferentiated progenitors) and the acquisition of a highly branched, O4-immunoreactive phenotype (a marker for late, differentiating progenitors and early oligodendrocytes). Only cells with silencedHDAC1 orHDAC2, not those with silenced HDAC3 orHDAC8, showed defective differentiation (Fig. 8c). Together, these data support a critical role of specific class I HDAC isoforms in oligodendrocyte differentiation and suggest that their levels and recruitment to specific promoter regions is important for the modulation of a concerted program of gene expression during remyelination.

From this cumulative evidence, we conclude that differences in remyelination efficiency between young and old mice are the consequence of inefficient epigenetic regulation of gene expression leading to a dysregulated transcriptional response (Supplementary Fig. 7 online). These differences create a cellular context that is characterized by altered transcriptional programs of OPC differentiation during remyelination in aged mice and hence to an impairment of this key regenerative process.

DISCUSSION

The concept that the adult neural stem or precursor cell population might be better harnessed to regenerate neural tissue after neurological disease is the subject of increasing interest and attention within the neurosciences[34]. After pathological processes characterized by myelin damage, there can be a highly effective regenerative process, in which a population of adult neural stem or progenitor cells, OPCs, is rapidly activated andmobilized to generate newmyelinating oligodendrocytes[3].

Although recent studies indicate the presence of extensive remyelination in the CNS of subjects with multiple sclerosis, they also illustrate that remyelination is not an inevitable consequence of demyelination and that axons can persist in a chronically demyelinated state, in which they are vulnerable to atrophy[6,7]. Thus, promoting remyelination remains an important therapeutic objective. As a proportion of non-remyelinating lesions in multiple sclerosis contain OPCs that fail to differentiate into myelinating oligodendrocytes, an understanding of the mechanisms which govern OPC differentiation will be crucial to this endeavor. An explanation that has attracted some attention is that such lesions contain remyelination inhibitors such as PSA-NCAM[35], hyaluronan[36] and Notch ligands[37], although the significance of the last is unclear[38]. An alternative explanation is that the process fails because of defects in inducers of differentiation, both environmental and cell intrinsic. An important clue to understanding failed repair in multiple sclerosis lesions is provided by the observation that remyelination, like all other regenerative processes, declines in efficiency with aging. Age-associated changes in the environmental signals associated with remyelination have been described in experimental models. However, although it is clear that cell-intrinsic changes occur in OPC biology with aging[39], the intrinsic mechanisms regulating OPC differentiation during remyelination remained unexplored.

In this manuscript, we define the age-dependent differences in intrinsic mechanisms of remyelination efficiency by focusing on the epigenome, a critical component at the interface between environmental signals and coordinated transcriptional programs regulating oligodendrocyte differentiation and myelin gene expression. The epigenome defines the entirety of the components affecting gene expression, including nucleosomal histones, DNA methylation and ATP remodeling complexes. The importance of epigenetics during differentiation has been shown in many lineages. In the oligodendroglial lineages, the importance of histone deacetylation for OPC differentiation has been supported by a large series of experiments *in vitro*[40,41] and *in vivo*[24,25,27,42]. Pharmacological inhibitors of HDAC have also been implicated in preventing the downregulation of neural stem cells markers in cultured OPCs[26]. The results of this study identify the epigenetic modulation of transcriptional inhibitors as a critical determinant of remyelination efficiency in young and old mice.

Using the cuprizone model of demyelination, we have shown here that spontaneous remyelination is characterized by the execution of a coordinated and integrated transcriptional response defined by the downregulation of the stem cell marker *Sox2* and of the oligodendrocyte differentiation inhibitors *Hes5, Hes1, Id2* and *Id4* before the upregulation of the transcription factor Olig1 and subsequent increase in myelin gene expression. Hes5 is highly expressed in proliferating OPCs but gradually decreases as the cells mature into oligodendrocytes[29]. Several direct and indirect mechanisms have been characterized to explain the role of Hes5 as inhibitor of myelin gene expression[43]. It has also been shown that Hes5 and its upstream Notch receptor are expressed in immature oligodendrocytes around active multiple sclerosis plaques but not within the remyelinated lesions[37]. However, genetic manipulation of Notch signaling pathway does not affect remyelination efficiency[38], indicating either that Notch signaling is critical but not rate limiting during the remyelination process or that the remyelination process may be affected by multiple pathways and other transcription factors. A potential candidate gene for affecting repair is *Sox2*, a transcription factor involved in stem cell pluripotency[26]. We show here that *Sox2* is also regulated by age-dependent mechanisms of histone acetylation and HDAC1 and HDAC2 recruitment to the promoter region during the remyelination process. Although the role of Sox2 as inhibitor of myelin gene expression has not been characterized, it is tempting to speculate that its function in the oligodendrocyte lineage might be equivalent to the one described in the peripheral nervous system, where it acts as inhibitor of Schwann cell differentiation and myelination[44].

The coordinated decrease of multiple inhibitory transcripts is detected only in young mice, not in old, and is characterized by the recruitment of several HDAC isoforms to the promoter with consequent deacetylation of lysine residues in histone H3 and release of RNA Pol II. With aging, this intrinsic ability of the cells to recruit HDAC to the promoter of transcriptional inhibitors progressively decreases. As a consequence, the intracellular environment of aged OPC is poised against differentiation because of the persistence of high levels of transcriptional inhibitors.

The identification of several nuclear HDAC isoforms at the promoter region of *Hes5* or *Sox2* suggested that multiple HDAC isoforms are involved in repressing differentiation inhibitors and ensure the initiation of the repair process. To define the role of specific HDAC isoforms, we pursued a silencing approach and individually targeted the distinct isoforms of class I HDAC, which we previously showed to be the prominent nuclear HDACs in oligodendrocyte-lineage cells[27]. It is noteworthy that silencing of HDAC1 or HDAC2, but not HDAC3 or HDAC8, impaired the timely differentiation of oligodendrocyte progenitor. Cells with decreased HDAC1 or HDAC2 retained the morphological and antigenic characteristics of early progenitors and showed high Sox2 levels. Thus, we conclude that the levels of HDAC1 and HDAC2 isoforms are critical for the execution of a timely program of oligodendrocyte differentiation. We also addressed the role of HDAC activity in repressing differentiation inhibitors, using a broad-spectrum pharmacological approach *in vitro* and *in vivo*. The effect of HDAC inhibitors (HDACi) in cultured cells was notably cell specific, as it increased the levels of *Sox2* and *Hes5* in primary cultures of OPCs but not astrocytes or microglia. This effect was accompanied by a significant reduction of myelin gene expression in treated OPCs, whereas we observed no reduction in microglial or astrocytic genes. Inhibition of HDAC activity *in vivo* significantly hampered remyelination in the brains of young mice, resulting in substantially fewer myelinated fibers and higher levels of inhibitors, thereby recreating an environment that mimicked the inefficient repression detected in the old brains. Together, these data define the epigenetic control of transcription as a critical determinant of remyelination efficiency in young mice and of remyelination inefficiency in old mice.

The use of HDACi for therapeutic purposes is the subject of an intensive debate. HDACi are at present used as anti-cancer agents because the are able to increase genes involved in growth arrest and promote apoptosis of cancer cells[45]. The possibility of using HDACi in demyelinating disorders is more controversial. Some studies have reported a beneficial effect of compounds increasing histone acetylation in mice with experimental allergic encephalomyelitis[46], whereas others have reported a beneficial effect of compounds increasing histone deacetylation in the same inflammatory model of demyelination[47]. The clinical improvement in mice treated with compounds increasing histone acetylation was ascribed to increased expression of protective genes[46] and possibly to the apoptosis of inflammatory cells[48]. The protective effect of increased histone deacetylation, in contrast, was proposed to be due to decreased expression of proinflammatory genes in T cells[46].

Our study contributes to the debate on the therapeutic potential of HDACi by analyzing a model of demyelination in the absence of the adaptive immune response and suggests that inhibition of HDAC might bear negative consequences for the repair process regardless of its effect on the immune cells. Using the cuprizone model of demyelination consequent to oligodendrogliopathy, we show here that retaining high levels of acetylated histones during remyelination significantly impairs the repair process.

In conclusion, this study defines the age-dependent decline in spontaneous remyelination as the result of the progressive loss of the epigenetic events modulating a coordinated program of gene expression. In addition, it defines the limitations of a pharmacological approach using broad inhibitors and proposes the identification of more specific molecular targets that require

further exploration for the possible development of cell-specific therapies aimed at ageappropriate brain repair.

METHODS

Antibodies

See Supplementary Methods online.

Cell culture and treatment

Oligodendrocyte progenitors were isolated from the cortex of postnatal day (P) 1 rats and cultured as described previously[24]. Primary astrocytes were collected from flasks by trypsinization, after the third shake-off, and were cultured in DMEM (Gibco) supplemented with 20% FBS (Gibco) and antibiotics. Either microglial cells were isolated by fast shake-off for 15 min from mixed glial cultures or immortalized microglial cells (the BV-2 cell line) were used. Both cultures were maintained in DMEM/F12 (Gibco) supplemented with 10% FBS. Cuprizone treatment (25 μM) in the presence or absence of VPA (1 mg ml^{-1}) was performed for 24 h in all cell types. For differentiating progenitors, the treatment was performed in proliferating conditions and during the first 24 h of differentiation.

Experimental induction of demyelination by cuprizone diet

Male 8-week-old (young) or 10-month-old (old) mice were purchased from Jackson Laboratory and placed on a diet of cuprizone mixed into chow pellets (Harlan Teklad Certified LM-485 code 7012CM). Young and old mice were subject to a 0.2% or 0.4% (wt/wt) cuprizone diet[28] according to well-defined protocols[31]. Sham- and cuprizone-treated mice were maintained on the cuprizone diet until the appropriate time point or, for the time-course study, killed weekly. In some cases, mice were returned to normal chow pellets for 2 weeks after the 6-week cuprizone diet. Mice were maintained in sterile, pathogen-free conditions under protocols approved by the Institutional Animal Care and Use Committee of Robert Wood Johnson Medical School, University of Medicine and Dentistry of New Jersey.

VPA injection

The first group of C57BL/6 mice were injected daily with saline ($n \geq 6$) or VPA ($n \geq 6$) (300 mg per kilogram body weight) at the beginning of the cuprizone diet. After 4 weeks of continuous feeding and VPA administration, mice were killed for RNA or protein harvesting ($n \geq 3$ for saline or VPA treatment, respectively) or perfused with 4% PFA for immunohistochemical analysis ($n \geq 3$ for saline or VPA treatment, respectively).

The second group of C57BL/6 mice were injected daily with saline ($n \geq 6$) or VPA ($n \geq 6$) (300 mg kg^{-1}) starting from the third week of the cuprizone diet and lasting until the end of the experiment. Mice were then perfused for immunohistochemical analysis or electronic microscopy. P4 neonatal pups received daily subcutaneous injection of either saline ($n = 6$) or VPA (300 mg kg^{-1}; $n = 6$) until P14 and then used as a source of chromatin to confirm the results obtained in the adult mice.

Immunohistochemistry

Mice were anesthetized and then perfused with 4% PFA in 0.1 M phosphate buffer. Brains were removed from the skulls, postfixed, cryopreserved in 30% sucrose, embedded in OCT and sectioned coronally (20 μm). Frozen sections were permeabilized with blocking buffer (0.1 M phosphate buffer, 5% normal goat serum (Vector Laboratories) and 0.5% Triton X-100). Incubation with primary antibodies was performed overnight at 21–24 °C (see Antibodies section for sources and dilutions). After 1 h incubation with secondary antibodies, either

directly conjugated to specific fluorochromes (whole Ig-Cy3, 1:200; Sigma-Aldrich) or biotinylated (RPN-1004, 1:200; Amersham Biosciences), the sections were counterstained with DAPI (1:1,000; Molecular Probes) in the absence or presence of avidin-conjugated fluorescein isothiocyanate (FITC) or Texas Red (RPN-1232 and RPN-1233, diluted 1:500; Amersham Biosciences). Stained sections were visualized using an inverted fluorescence microscope (DM RA; Leica) and confocal microscopy (LSM510Meta confocal laser scanning microscope; Zeiss). Pinhole diameters of 123 μm, 126 μm and 124 μm were used with the ×63 objective for the rhodamine, DAPI and FITC channels, respectively. The thickness of the optical slices was 1 μm, and stacks of seven were typically used to generate the projections. In quantifying confocal images from distinct groups of treatment, the same tissue depth and number of optical sections were used. NIH ImageJ software was used to measure Sox2 nuclear intensity in confocal images.

Quantification of axonal damage

To identify the potential effect of the cuprizone dose and VPA treatment on axonal damage in the corpus callosum, we identified transected axons by staining axonal spheroids with an antibody that specifically recognizes unphosphorylated neurofilament heavy chain (SMI-32, Sternberger Monoclonals). We stained frozen coronal sections of the posterior corpus callosum from young (8-week-old) and aged (10-month-old) mice treated with different doses of cuprizone. Different age and treatment groups were analyzed: saline treated and VPA treated young mice on a 0.2% cuprizone diet and young and old mice on a 0.4% cuprizone diet for 4 weeks. To avoid nonspecific binding of antibody, we use a 1:500,000 dilution of the SMI-32 antibody for immunohistochemical analysis. The number of SMI-32$^+$ axonal spheroids was counted according to the criteria set by Blakemore[31] within the lateral and medial corpus callosum for each group. For each treatment and age group, at least three mice were used and at least six counts were obtained in each brain region from different fields of view. The axonal spheroid counts within the lateral and medial regions were compared using a two-tailed *t*-test.

Western blot analysis

Upon carefully removing the skin over the skull, the positions of the bregma and lambda sutures were marked on the brain surface. These positions were used as a reference point in dissecting out the same regions of corpus callosum from experimental mice. A coronal slice around the bregma was dissected out, and the corpus callosum was excised under a dissection microscope (Nikon) and used for either protein or RNA extraction. Tissue lysates from freshly dissected corpus callosum were prepared as previously described[27,30]. Western blot analysis was performed as reported previously[43], using the appropriate dilutions of primary and secondary antibodies (see Supplementary Methods for details). The immunoreactive bands were detected by ECL Plus Western Blotting Detection System (Amersham Biosciences). Equal protein loading was guaranteed by probing the blots with antibody to actin.

Densitometric analysis

Densitometry of the western blot protein bands was analyzed using NIH ImageJ Software. The density of the actin bands was used to standardize the density of class I HDAC protein expression at various treatment stages.

Quantitative RT-PCR

RNA was isolated using Trizol reagent and cleaned using RNeasy Mini kit (Qiagen). Two micrograms of total RNA was used in 20 ml of reverse transcription reaction, using SuperScript RT-PCR kit (Invitrogen). Quantitative real time PCR was performed using Applied Biosystems SYBR green PCR master mix in 7900HT Sequence Detection PCR System. The melting curve of each sample was measured to ensure the specificity of the products. Data were normalized

to the internal control *Gapdh* and analyzed using Pfaffl ΔΔ*Ct* method. Primers used in quantitative PCR for mouse are given in Supplementary Methods.

Electron microscopy

Mice were deeply anesthetized with a 2.5% solution of 2,2,2-tribromoethanol (Sigma-Aldrich) and transcardially perfused with 0.9% NaCl followed by a 0.1 M Millonig's solution containing 4% formaldehyde and 5% glutaraldehyde, pH 7.3 ref. (49). After postfixation for 2 weeks in the same solution, samples from corpus callosum at the level of the fornix were harvested and processed for standard transmission electron microscopic analysis as previously described[49]. One-micron sections stained with toluidine blue and ultrathin sections stained with uranyl acetate and lead citrate were used for myelin structural analysis using a Jeol JEM1230 transmission electron microscope equipped with a Gatan Ultrascan 4000SP 4K×4K CCD camera. For quantitative analysis, a minimum of ten micrographs per tissue sample from each mouse, taken at × 5,000, were collected. From these images, the percentage of myelinated axons was determined by counting the total number of axons with diameters larger than 0.3 microns. An axon was classified as myelinated if it showed a complete wrap of an oligodendrocyte process. G ratios were calculated by dividing axon diameter by the diameter of the entire myelinated fiber. A minimum of 40 myelinated axons per mouse were used to compare myelin thickness. Healthy axons were defined on the basis of the presence of intact membranes and the normal complement of organelles, including empty vesicles, neurofilaments and microtubules. Further criteria included the presence of mitochondria and the integrity of the cristae. Degenerating or unhealthy axons were characterized by the presence of mitochondria lacking cristae, dark and frequently amorphous vesicles and the presence of clumped cytoskeletal components.

Chromatin immunoprecipitation

Chromatin was isolated from tissue or cells, cross-linked, immunoprecipitated using 2 μg of antibody (Supplementary Methods) and then reversed cross-linked using EZ ChIP kit (Upstate Biotechnology). Proteins were digested with proteinase K, and the recovered DNA was purified using QIAGEN QIAquick PCR purification kit and subjected either to quantitative PCR or semiquantitative PCR amplification as previously described[42]. ChIP from cells was performed following a modified Q^2 protocol[50]. Primers used for ChIP in are given in the Supplementary Methods. DNA recovered from chromatin that was not immunoprecipitated (input) and chromatin that was immunoprecipitated with either protein A or protein G in the absence of primary antibody were used as controls.

Silencing experiments

Immunoselected primary cortical oligodendrocyte progenitors were seeded at a density of 2×10^4 cells into eight-well chamber slides for experimental treatment. Cells were transfected with either control (siGLO RISC-Free Control siRNA, D-001600-01-05) or Smartpool HDAC siRNA (rat HDAC1, On-target Plus, L-084421-00; rat HDAC2, On-target Plus, L-093064-00; rat HDAC3, On-target Plus, L-093064-00; rat HDAC8, Accell Smartpool, E-096589-00). The final concentration of 25 nM siRNA was mixed with transfection reagents from Mirus (TransIT-TKO, MIR-2154), and 30 min later, the mixture was added dropwise to the cells. Four hours after transfection, medium was changed and cells were maintained in growth medium for 1 d. Forty-eight hours after transfection, cells were deprived of growth factors and grown in medium for additional 4 d. To examine the effect of silencing HDACs on OPC differentiation, cells were stained live with the A2B5 and the O4 antibodies, then fixed with 4% PFA and processed for immunocytochemistry.

Statistical methods

Results are expressed as mean ± s.d. and were statistically analyzed using two-tailed Student's *t*-tests. A P value of < 0.05 was considered statistically significant.

Supplementary Material

Refer to Web version on PubMed Central for supplementary material.

ACKNOWLEDGMENTS

This work was supported by grants from US National Institutes of Health National Institute of Neurological Disorders and Stroke (NS042925 and NS52738 to P.C.-B.), the National Multiple Sclerosis Society (NMSS RG-3957 P.C.-B.), the MS Research Foundation (to P.C.-B.) and Research into Ageing (to R.J.M.F.). We thank J. Williamson for superb assistance with electron microscopy and acknowledge C. Ghiani (University of California Los Angeles) for the gift of the microglial BV-2 cell line.

References

1. Gensert JM, Goldman JE. Endogenous progenitors remyelinate demyelinated axons in the adult CNS. Neuron 1997;19:197–203. [PubMed: 9247275]
2. Dawson MR, et al. NG2-expressing glial progenitor cells: an abundant and widespread population of cycling cells in the adult rat CNS. Mol. Cell. Neurosci 2003;24:476–488. [PubMed: 14572468]
3. Zhao C, et al. Stem cells, progenitors and myelin repair. J. Anat 2005;207:251–258. [PubMed: 16185249]
4. Blakemore WF. Remyelination of the superior cerebellar peduncle in the mouse following demyelination induced by feeding cuprizone. J. Neurol. Sci 1973;20:73–83. [PubMed: 4744512]
5. Woodruff RH, Franklin RJM. The expression of myelin protein mRNAs during remyelination of lysolecithin-induced demyelination. Neuropathol. Appl. Neurobiol 1999;25:226–235. [PubMed: 10417664]
6. Patrikios P, et al. Remyelination is extensive in a subset of multiple sclerosis patients. Brain 2006;129:3165–3172. [PubMed: 16921173]
7. Patani R, et al. Remyelination can be extensive in multiple sclerosis despite a long disease course. Neuropathol. Appl. Neurobiol 2007;33:277–287. [PubMed: 17442065]
8. Albert M, et al. Extensive cortical remyelination in patients with chronic multiple sclerosis. Brain Pathol 2007;17:129–138. [PubMed: 17388943]
9. Franklin RJM. Why does remyelination fail in multiple sclerosis? Nat. Rev. Neurosci 2002;3:705–714. [PubMed: 12209119]
10. Dubois-Dalcq M, et al. Enhancing central nervous system remyelination in multiple sclerosis. Neuron 2005;48:9–12. [PubMed: 16202704]
11. Miller RH, Mi S. Dissecting demyelination. Nat. Neurosci 2007;10:1351–1354. [PubMed: 17965654]
12. Shields SA, et al. Remyelination occurs as extensively but more slowly in old rats compared to young rats following gliotoxin-induced CNS demyelination. Glia 1999;28:77–83. [PubMed: 10498825]
13. Li WW, et al. Females remyelinate more efficiently than males following demyelination in the aged but not young adult CNS. Exp. Neurol 2006;202:250–254. [PubMed: 16797535]
14. Sim FJ, et al. The age-related decrease in CNS remyelination efficiency is attributable to an impairment of both oligodendrocyte progenitor recruitment and differentiation. J. Neurosci 2002;22:2451–2459. [PubMed: 11923409]
15. Woodruff RH, et al. Platelet-derived growth factor regulates oligodendrocyte progenitor numbers in adult CNS and their response following CNS demyelination. Mol. Cell. Neurosci 2004;25:252–262. [PubMed: 15019942]
16. Wolswijk G. Oligodendrocyte regeneration in the adult rodent CNS and the failure of this process in multiple sclerosis. Prog. Brain Res 1998;117:233–247. [PubMed: 9932412]
17. Chang A, et al. NG2-positive oligodendrocyte progenitor cells in adult human brain and multiple sclerosis lesions. J. Neurosci 2000;20:6404–6412. [PubMed: 10964946]

18. Chang A, et al. Premyelinating oligodendrocytes in chronic lesions of multiple sclerosis. N. Engl. J. Med 2002;346:165–173. [PubMed: 11796850]
19. Hinks GL, Franklin RJM. Delayed changes in growth factor gene expression during slow remyelination in the CNS of aged rats. Mol. Cell. Neurosci 2000;16:542–556. [PubMed: 11083917]
20. Zhao C, et al. Differences in the early inflammatory responses to toxin-induced demyelination are associated with the age-related decline in CNS remyelination. Neurobiol. Aging 2006:1298–1307. [PubMed: 16051398]
21. O'Leary MT, et al. Increasing local levels of IGF-I mRNA expression using adenoviral vectors does not alter oligodendrocyte remyelination in the CNS of aged rats. Mol. Cell. Neurosci 2002;19:32–42. [PubMed: 11817896]
22. Arnett HA, et al. bHLH transcription factor Olig1 is required to repair demyelinated lesions in the CNS. Science 2004;306:2111–2115. [PubMed: 15604411]
23. Gokhan S, et al. Combinatorial profiles of oligodendrocyte-selective classes of transcriptional regulators differentially modulate myelin basic protein gene expression. J. Neurosci 2005;25:8311–8321. [PubMed: 16148239]
24. Liu A, et al. The glial or neuronal fate choice of oligodendrocyte progenitors is modulated by their ability to acquire an epigenetic memory. J. Neurosci 2007;27:7339–7343. [PubMed: 17611286]
25. He Y, et al. The transcription factor Yin Yang 1 is essential for oligodendrocyte progenitor differentiation. Neuron 2007;55:217–230. [PubMed: 17640524]
26. Lyssiotis CA, et al. Inhibition of histone deacetylase activity induces developmental plasticity in oligodendrocyte precursor cells. Proc. Natl. Acad. Sci. USA 2007;104:14982–14987. [PubMed: 17855562]
27. Shen S, et al. Histone modifications affect timing of oligodendrocyte progenitor differentiation in the developing rat brain. J. Cell Biol 2005;169:577–589. [PubMed: 15897262]
28. Matsushima GK, Morell P. The neurotoxicant, cuprizone, as a model to study demyelination and remyelination in the central nervous system. Brain Pathol 2001;11:107–116. [PubMed: 11145196]
29. Kondo T, Raff M. Basic helix-loop-helix proteins and the timing of oligodendrocyte differentiation. Development 2000;127:2989–2998. [PubMed: 10862737]
30. Shen S, et al. Epigenetic memory loss in aging oligodendrocytes in the corpus callosum. Neurobiol. Aging 2008;29:452–463. [PubMed: 17182153]
31. Irvine KA, Blakemore WF. Age increases axon loss associated with primary demyelination in cuprizone-induced demyelination in C57BL/6 mice. J. Neuroimmunol 2006;175:69–76. [PubMed: 16626812]
32. Mason JL, Langaman C, Morell P, Suzuki K, Matsushima GK. Episodic demyelination and subsequent remyelination within the murine central nervous system: changes in axonal calibre. Neuropathol. Appl. Neurobiol 2001;27:50–58. [PubMed: 11299002]
33. Zhao C, Li WW, Franklin RJM. Differences in the early inflammatory responses to toxin-induced demyelination are associated with the age-related decline in CNS remyelination. Neurobiol. Aging 2006;27:1298–1307. [PubMed: 16051398]
34. Lindvall O, Kokaia Z. Stem cells for the treatment of neurological disorders. Nature 2006;441:1094–1096. [PubMed: 16810245]
35. Charles P, et al. Re-expression of PSA-NCAM by demyelinated axons: an inhibitor of remyelination in multiple sclerosis? Brain 2002;125:1972–1979. [PubMed: 12183343]
36. Back SA, et al. Hyaluronan accumulates in demyelinated lesions and inhibits oligodendrocyte progenitor maturation. Nat. Med 2005;11:966–972. [PubMed: 16086023]
37. John GR, et al. Multiple sclerosis: re-expression of a developmental pathway that restricts oligodendrocyte maturation. Nat. Med 2002;8:1115–1121. [PubMed: 12357247]
38. Stidworthy MF, et al. Notch1 and Jagged1 are expressed after CNS demyelination, but are not a major rate-determining factor during remyelination. Brain 2004;127:1928–1941. [PubMed: 15289265]
39. Tang DG, et al. Long-term culture of purified postnatal oligodendrocyte precursor cells. Evidence for an intrinsic maturation program that plays out over months. J. Cell Biol 2000;148:971–984. [PubMed: 10704447]

40. Marin-Husstege M, et al. Histone deacetylase activity is necessary for oligodendrocyte lineage progression. J. Neurosci 2002;22:10333–10345. [PubMed: 12451133]
41. Liu A, et al. Oligodendrocyte process outgrowth in vitro is modulated by epigenetic regulation of cytoskeletal severing proteins. Glia 2003;44:264–274. [PubMed: 14603467]
42. Hsieh J, et al. Histone deacetylase inhibition-mediated neuronal differentiation of multipotent adult neural progenitor cells. Proc. Natl. Acad. Sci. USA 2004;101:16659–16664. [PubMed: 15537713]
43. Liu A, et al. A molecular insight of Hes5-dependent inhibition of myelin gene expression: old partners and new players. EMBO J 2006;25:4833–4842. [PubMed: 17006542]
44. Le N, et al. Analysis of congenital hypomyelinating Egr2Lo/Lo nerves identifies Sox2 as an inhibitor of Schwann cell differentiation and myelination. Proc. Natl. Acad. Sci. USA 2005;102:2596–2601. [PubMed: 15695336]
45. Marks PA, et al. Inhibitors of histone deacetylase are potentially effective anticancer agents. Clin. Cancer Res 2001;7:759–760. [PubMed: 11309319]
46. Camelo S, et al. Transcriptional therapy with the histone deacetylase inhibitor trichostatin A ameliorates experimental autoimmune encephalomyelitis. J. Neuroimmunol 2005;164:10–21. [PubMed: 15885809]
47. Natarajan C, Bright JJ. Curcumin inhibits experimental allergic encephalomyelitis by blocking IL-12 signaling through Janus kinase-STAT pathway in T lymphocytes. J. Immunol 2002;168:6506–6513. [PubMed: 12055272]
48. Chen PS, et al. Valproic acid and other histone deacetylase inhibitors induce microglial apoptosis and attenuate lipopolysaccharide-induced dopaminergic neurotoxicity. Neuroscience 2007;149:203–212. [PubMed: 17850978]
49. Dupree JL, et al. Galactolipids in the formation and function of the myelin sheath. Microsc. Res. Tech 1998;41:431–440. [PubMed: 9672425]
50. Dahl JA, Collas P. Q2ChIP, a quick and quantitative chromatin immunoprecipitation assay unravels epigenetic dynamics of developmentally regulated genes in human carcinoma cells. Stem Cells 2007;25:1037–1046. [PubMed: 17272500]

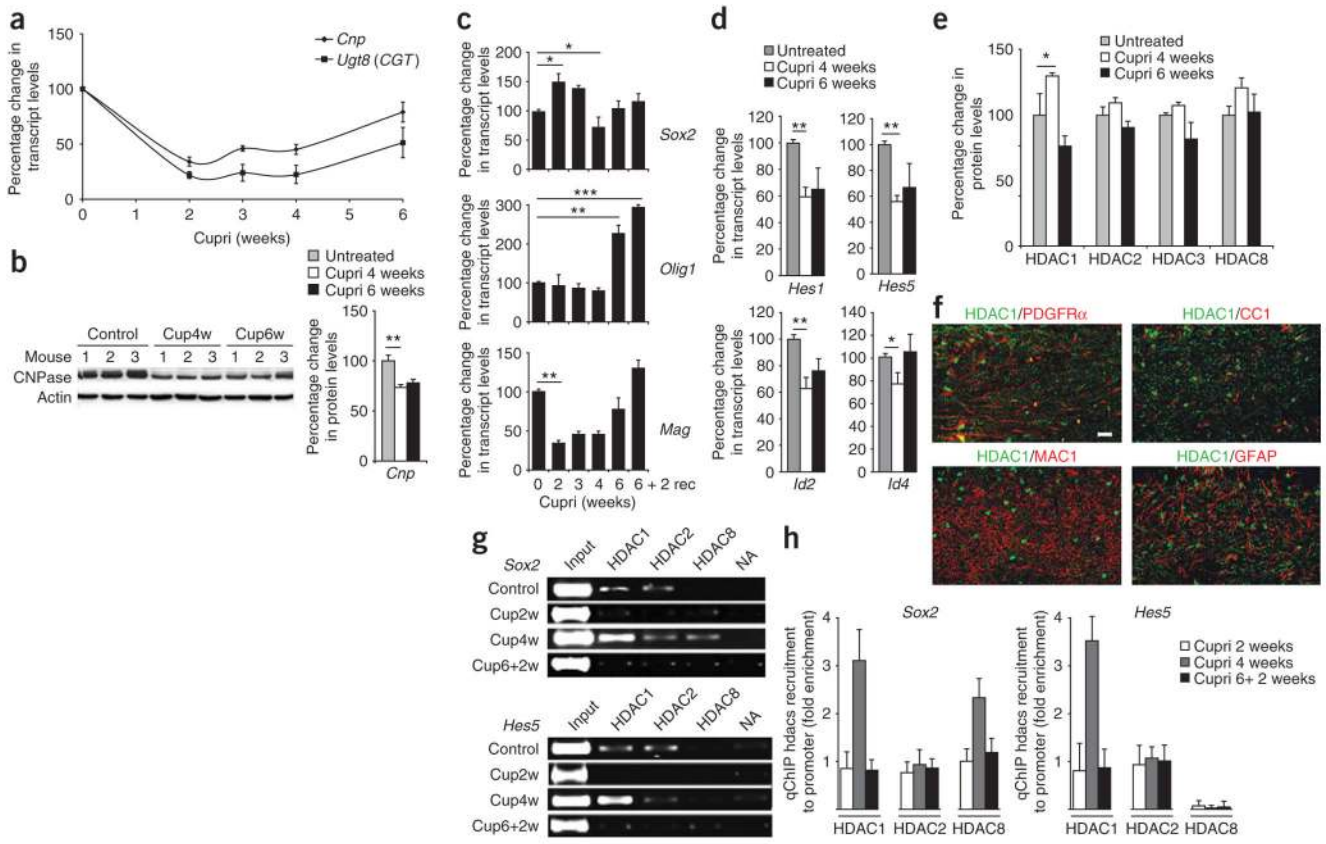

Figure 1.

Complex temporal pattern of regulation of gene expression in the corpus callosum of cuprizone-treated mice. (**a**) Levels of myelin gene transcripts in the corpus callosum of mice treated with cuprizone (cupri), measured by qRT-PCR and normalized to *Gapdh* ($n = 3$). (**b**) Western blot analysis of proteins extracted from the corpus callosum of individual mice at 4 weeks (Cup4w) or 6 weeks (Cup6w), quantified by densitometry and normalized to actin levels. (**c,d**) qRT-PCR of *Sox2, Olig1* and *Mag* (**c**) and *Hes1, Hes5, Id2* and *Id4* (**d**) in the corpus callosum of cuprizone-treated mice, normalized to *Gapdh* and expressed as percentage of the values in untreated mice ($n = 6$). (**e**) Levels of class1 HDAC proteins measured by western blot, quantified by densitometry and normalized to actin levels ($n = 3$; untreated, gray; 4 weeks cuprizone, white; 6 weeks cuprizone, black). In **a–e**, $*P < 0.05$, $**P < 0.01$, $***P < 0.001$; $n = 3$; error bars, s.d. (**f**) Confocal image of the dorsal corpus callosum in mice treated for 4 weeks with cuprizone, stained with antibodies for HDAC1 (green) and for specific cellular markers as indicated (red). Scale bar, 20 μm; ×25 objective. (**g**) ChIP of samples isolated from the corpus callosum of mice treated with cuprizone for the indicated time periods ($n = 8$) and immunoprecipitated with antibodies for HDAC1, HDAC2 and HDAC8. NA, no-antibody control; Cup6+2w, a 2-week recovery period after 6 weeks of cuprizone treatment. The immunoprecipitated DNA was amplified using specific primer pairs for the regions surrounding the *Sox2* and *Hes5* (**d**) promoters. (**h**) qChIP of chromatin prepared as described in **g** (error bars, s.d.; $n = 8$).

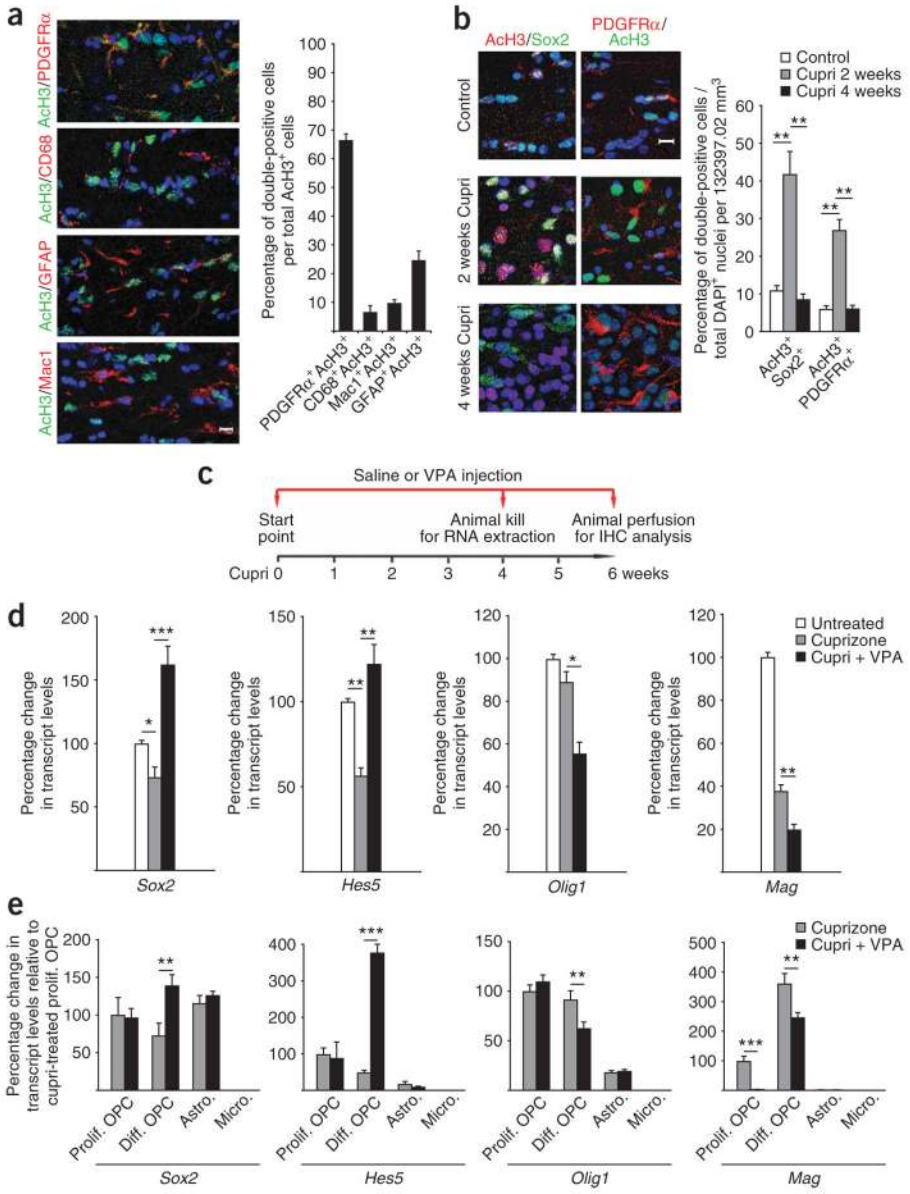

Figure 2.

The pattern of histone acetylation in oligodendrocyte progenitors in the corpus callosum of cuprizone-treated mice correlates with the expression profile of the stem cell marker Sox2 and of the differentiation inhibitor Hes5. (**a**) Left, confocal images of the corpus callosum of mice fed with cuprizone for 2 weeks ($n = 3$), stained for AcH3 (green) and for cell type specific markers (red). Scale bar, 10 μm; ×63 objective. Right, percentage of double-positive cells relative to the total number of AcH3$^+$ cells. (**b**) Left, confocal image of the dorsal corpus callosum in control and cuprizone (cupri)-treated mice stained with antibodies for AcH3 (red) and Sox2 (green) or for AcH3 (green) and PDGFRα (red). Scale bar, 10 μm; ×63 objective. Right, percentage of double-positive cells relative to the total number of DAPI$^+$ cells (**$P <$ 0.01; $n = 3$). (**c**) Diagram of the scheme of saline or VPA administration (red line) relative to cuprizone treatment duration (black line). (**d**) *Hes5, Sox2, Olig1* and *Mag* levels in the corpus callosum of treated mice, measured by qRT-PCR, normalized to *Gapdh* and expressed as

percentage of those in untreated mice. (**e**) qRTPCR analysis of the same transcripts in primary proliferating (prolif.) OPCs, differentiating (diff.) OPCs, astrocytes (astro.) and microglia (micro.), treated either with cuprizone or with cuprizone and VPA. Values were normalized to *Gapdh* and expressed as percentage of those in proliferating OPCs (*$P < 0.05$; **$P < 0.01$; ***$P < 0.001$; $n = 3$; error bars, s.d.).

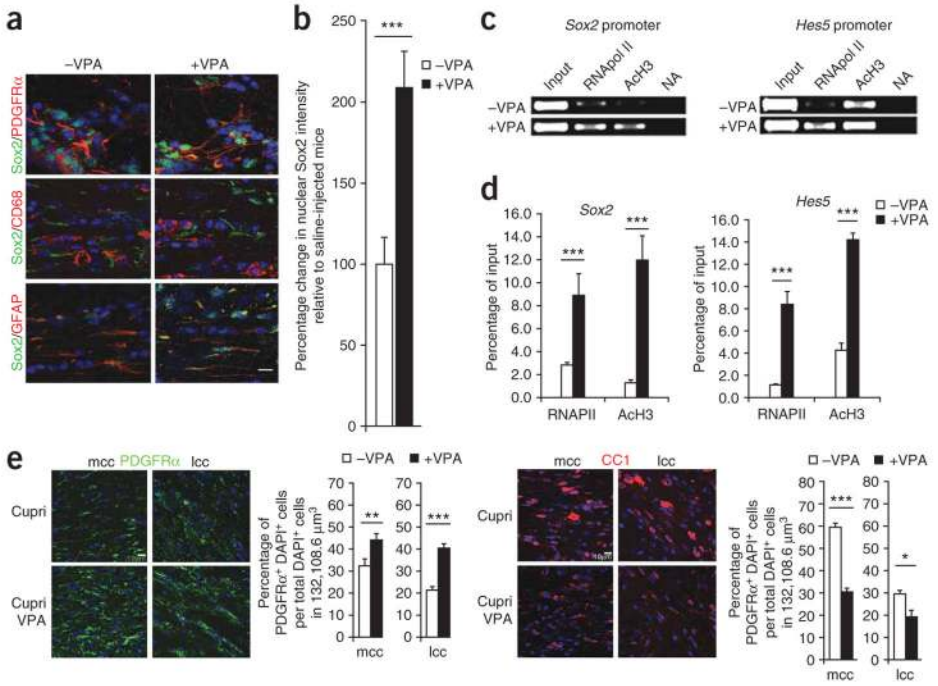

Figure 3.

Systemic administration of HDAC inhibitors to cuprizone-treated mice increases histone acetylation on the promoters of *Sox2* and *Hes5* and prevents oligodendrocytic differentiation. (**a**) Confocal images of the corpus callosum of mice treated as described in Figure 2c and stained with antibodies for Sox2 (green) and for cell type specific markers (red). Scale bar, 10 µm; ×63 objective. (**b**) Nuclear intensity of Sox2 protein fluorescence in PDGRα$^+$ cells in VPA treated mice normalized to the intensity detected in saline injected mice (***P <0.001; n = 60 cells; error bars, s.d.). (**c**) ChIP assay of the proximal region of *Sox2* and *Hes5* promoters in saline and VPA-treated mice immunoprecipitated with antibodies against active RNA polymerase II (RNApol II) and AcH3. Input DNA and sample without primary antibodies (NA) are shown as controls. (**d**) qChIP of the same region to assess the amount of RNA polymerase II (RNAPII) and of AcH3 binding (***P < 0.001; error bars, s.d.; n = 3). (**e**) Left, confocal images of the corpus callosum of mice treated with cuprizone (cupri) and either treated or not treated with VPA for 6 weeks, stained for PDGFRα (green) and CC1 (red). Scale bar, 10 µm; ×63 objective. Right, numbers of cells counted in the medial (mcc) and lateral (lcc) corpus callosum, normalized to the total number of DAPI$^+$ nuclei (*P < 0.05, **P < 0.01, ***P < 0.001; error bar, s.d.; n = 6 mice).

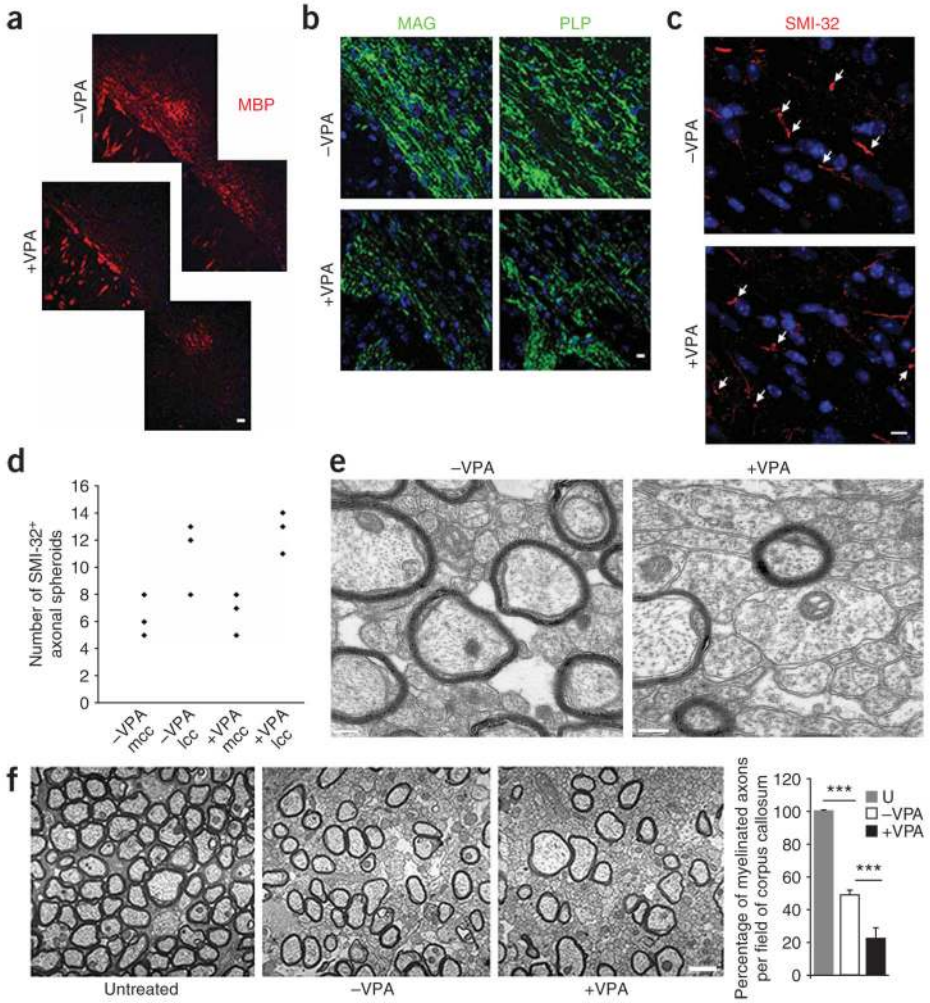

Figure 4.

The impaired remyelination detected in VPA-treated mice is not dependent on axonal damage. (**a–c**) Confocal images of the lateral corpus callosum of cuprizone mice treated with saline (−VPA) or VPA (+VPA), stained with antibodies for MBP (a), MAG and PLP (**b**) and hypophosphorylated neurofilament heavy chain (SMI-32, **c**). White arrows, SMI-32$^+$ axonal spheroids; DAPI (blue), nuclei. Scale bar, 10 μm; ×63 objective. (**d**) Scatter plot representation of SMI-32$^+$ axonal spheroids counted in the medial (mcc) and lateral (lcc) corpus callosum of salineor VPA-treated mice. (**e**) Electron micrograph showing the presence of many large-caliber myelinated axons in the corpus callosum of saline-but not VPA-treated mice after 6 weeks of cuprizone diet. Note that, despite the absence of myelin sheaths, the appearance of the small and large caliber axons in the VPA mice is very similar, with evenly spaced cytoskeletal elements and the presence of mitochondria with healthy cristae, indicating healthy axons. Scale bar, 200 nm. (**f**) Left, electron microscopy of the corpus callosum of mice either untreated or treated for 6 weeks with cuprizone and either saline or VPA. Scale bar, 1 μm. Right, quantification of the number of myelinated axons in the corpus callosum of untreated (U), saline-treated and VPA-treated mice (***$P < 0.001$; error bars, s.d.).

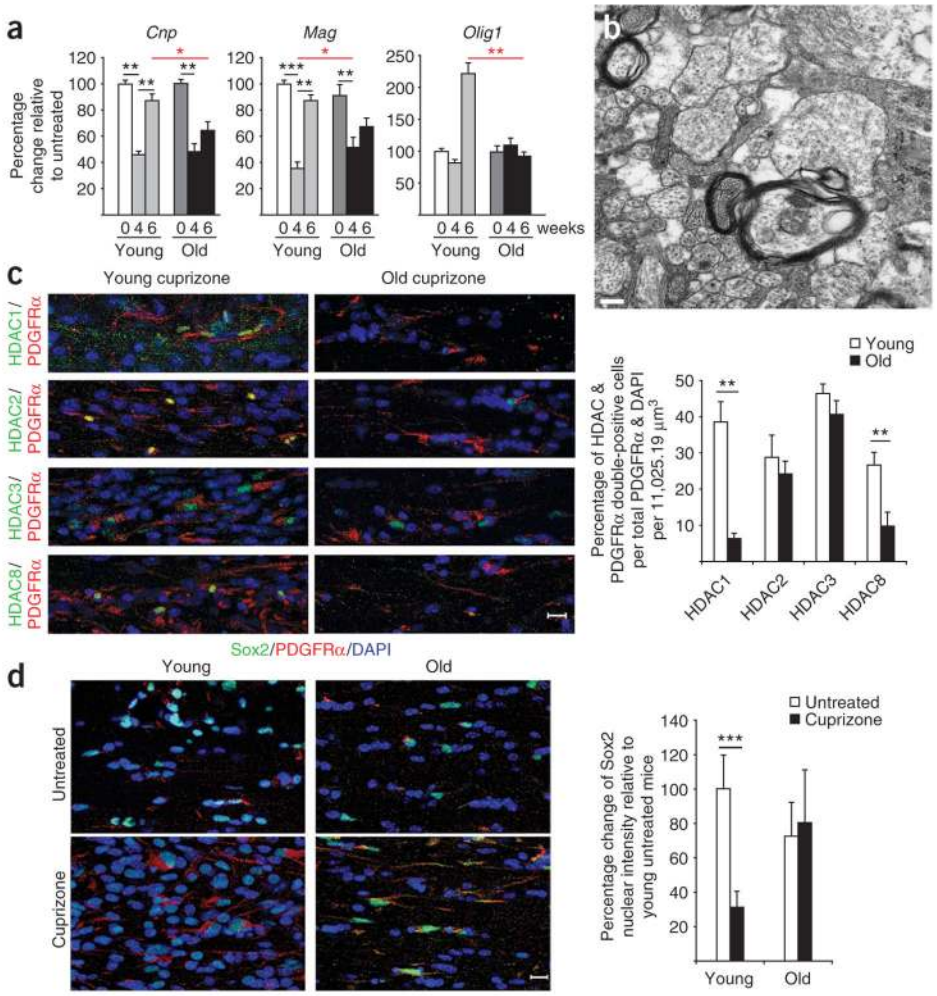

Figure 5.

Impaired recovery of myelin gene expression in old mice correlates with decreased number of HDAC$^+$ cells and increased number of Sox2$^+$ immature cells. (**a**) Transcript levels of *Cnp, Mag* and *Olig1* in the corpus callosum of young and old mice treated with cuprizone for the indicated time, measured by qRT-PCR and normalized to the levels in untreated mice of each age group (*P < 0.05; **P < 0.01; ***P < 0.001; n = 3). (**b**) Ultrastructure of unmyelinated axons in regions of the corpus callosum of old mice. Note the four axons that lack myelin even though they are of sufficient size for myelination (>0.3 μm) and healthy, as indicated by the presence of many cytoskeletal profiles and by the absence of axolemmal blebbing and electron-dense inclusions. Scale bar, 200 nm. (**c**) Left, confocal images of the corpus callosum of cuprizone-treated young and old mice stained for HDAC1, HDAC2, HDAC3 and HDAC8 (green); PDGFRα (red); and DAPI (blue). Scale bar, 10 μm; ×63 objective. Right, number of double-positive cells expressed as percentage of PDGFRα$^+$ cells (**P < 0.01). (**d**) Left, confocal images of the corpus callosum of young and old untreated or cuprizone-treated mice stained for Sox2 (green), PDGFRα (red) and DAPI (blue). Right, nuclear Sox2 intensity, normalized to levels in young, untreated mice (***P < 0.001; error bars, s.d.).

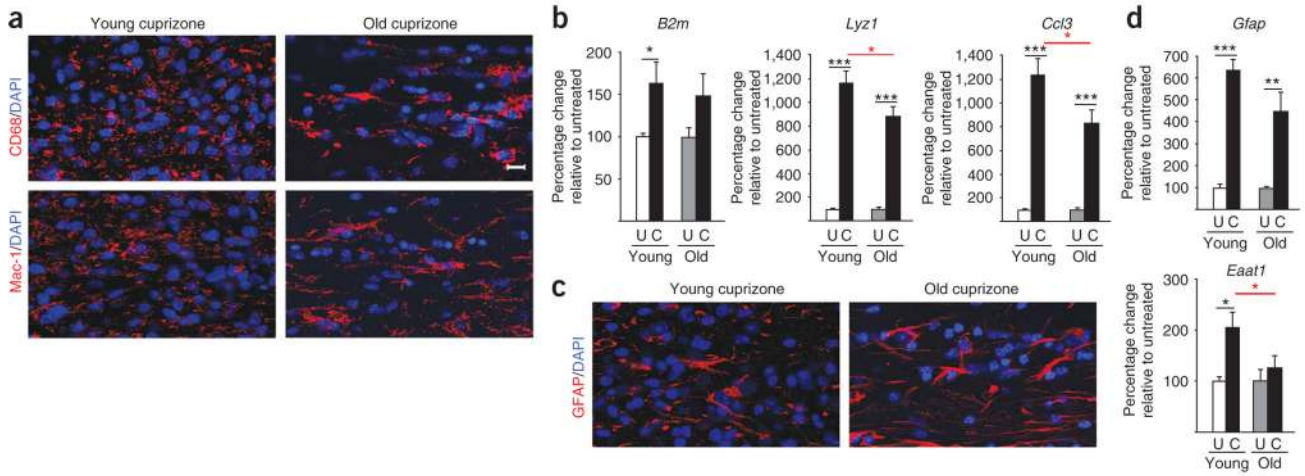

Figure 6.

The pattern of microglial and astrocytic gene expression is similar in the corpus callosum of young and old mice after cuprizone treatment. (**a**) Confocal images of corpus callosum of young and old mice either untreated or treated with cuprizone for 6 weeks, stained with CD68 (red) or Mac1 (red) to detect the macrophage or microglial population, respectively, and with DAPI (blue) for nuclei. Scale bar, 10 μm; ×63 objective. (**b**) Transcript levels of β-microglobulin (*B2m*), lysozyme (*Lyz1*) and chemokine ligand 3 (*Ccl3*) in the dorsal corpus callosum of young and old untreated (U) or cuprizone (C)-treated mice, measured by qRT-PCR, normalized to *Gapdh* and expressed relative to those in untreated mice of each age group. (**c**) Confocal images of the corpus callosum of young and old cuprizone-treated mice, stained with GFAP (red) and DAPI (blue). Scale bars, 10 μm, ×63 objective. (**d**) Transcript levels of *Gfap* and *Slc1a3 (Eaat1)*, measured by qRT-PCR, normalized to *Gapdh* and expressed relative to those in untreated mice of each age group. Black line, comparison between untreated and cuprizone treated; red line, comparison between young and old treated; **P* <0.05; ***P* < 0.01 and ****P* < 0.001; error bars, s.d.; *n* = 3 (**b,d**).

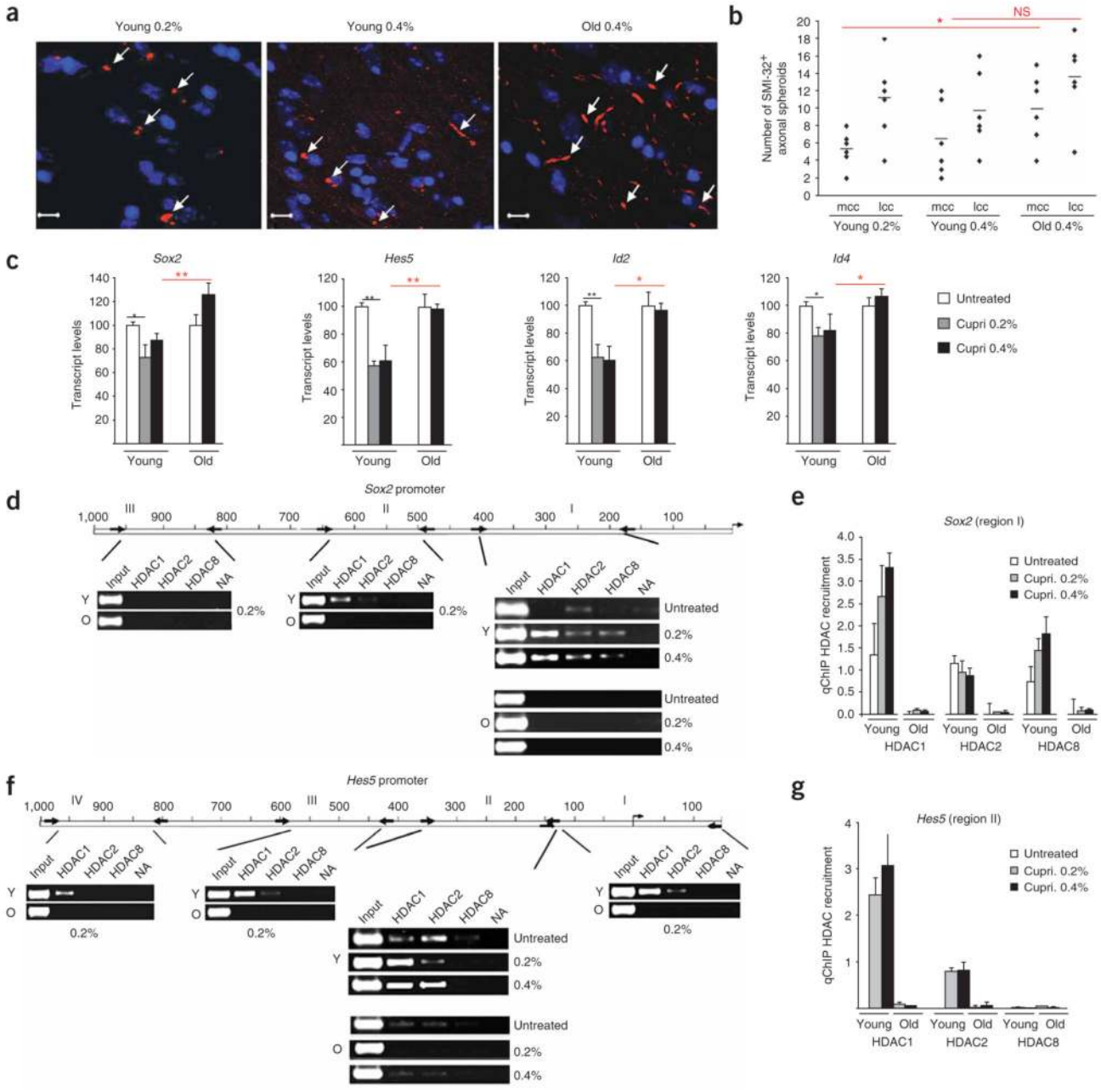

Figure 7.

Age-dependent and dose-independent recruitment of repressive complexes containing *HDAC* to *Hes5* and *Sox2* promoters during remyelination. (**a**) Confocal images of the lateral corpus callosum of mice of the indicated age and treatment with the indicated percentage of cuprizone, stained with SMI-32 (red) to identify axonal spheroids (white arrows) and with DAPI (blue). Scale bars, 10 μm. (**b**) Scatter plot of SMI-32$^+$ axonal spheroids counted in the medial (mcc) and lateral (lcc) corpus callosum of these mice (*$P < 0.05$; NS, not significant). (**c**) qRT-PCR analysis of *Sox2, Hes5, Id2* and *Id4* transcripts in young or old mice untreated or treated with 0.2% or 0.4% cuprizone (cupri.) for 4 weeks. Values were normalized to *Gapdh* and expressed relative to those in untreated mice (black line, comparison between

untreated and cuprizone treated; red line, comparison between young and old treated; *P < 0.05; **P < 0.01; error bars, s.d.; n = 3). (**d–g**) Recruitment of HDAC1, HDAC2 and HDAC8 to the indicated regions of the *Sox2* (**d**) and *Hes5* (**f**) promoters detected using ChIP on chromatin isolated from the corpus callosum of young (Y) and old (O) mice either untreated or treated for 4 weeks with the indicated doses of cuprizone (input and no antibody (NA) used as controls; n = 8). (**e,g**) Quantitative ChIP of region I of the *Sox2* promoter (**e**) and of region II of the *Hes5* promoter (**g**) in chromatin samples isolated from the corpus callosum of mice described in **d**. Bar graphs represent the enrichment of HDAC on the promoter regions relative to input DNA (error bars, s.d.).

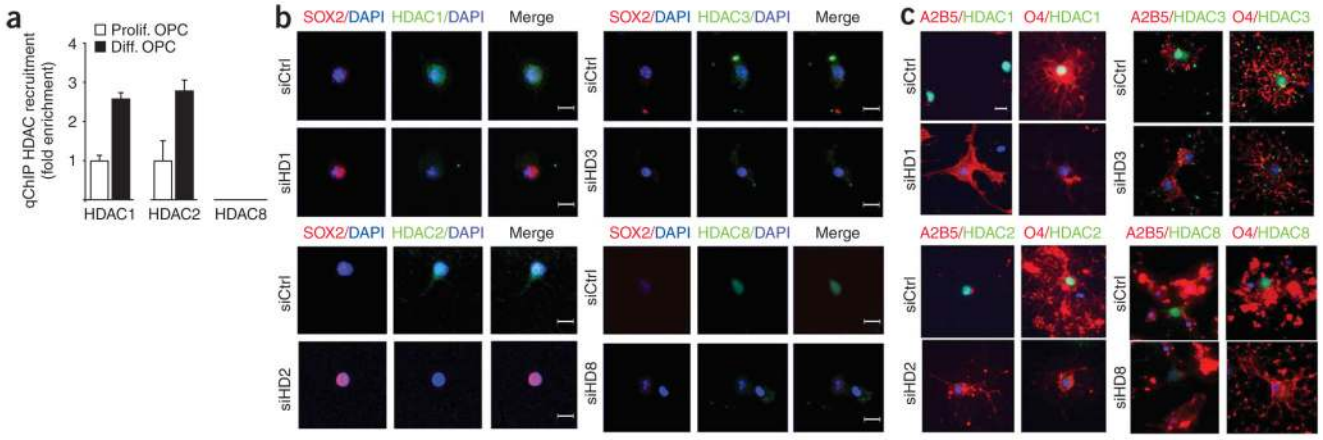

Figure 8.

Selective class I HDAC isoforms are necessary for oligodendrocyte progenitor differentiation and Sox2 downregulation. (**a**) ChIP assay of chromatin from proliferating (prolif.) and differentiating (diff.) primary OPCs immunoprecipitated with antibodies for HDAC1, HDAC2 and HDAC8 and analyzed with primers encompassing region I of the Sox2 promoter. Values expressed as fold increase in HDAC binding to *Sox2* promoter in differentiating compared to proliferating OPCs. (**b**) Confocal image of OPCs transfected with nontargeting siRNA (siCont) or siRNA targeting constructs specific for HDAC1 (siHD1), HDAC2 (siHD2), HDAC3 (siHD3) or HDAC8 (siHD8). After siRNA transfection, progenitors were allowed to differentiate for 3 d and were then stained with the appropriate HDAC antibody (green) to define the efficiency of silencing and with the Sox2 antibody (red). DAPI (blue) was used as nuclear counterstain. (**c**) Immunohistochemistry of OPCs transfected with siRNA constructs as described in **b** and then costained with the appropriate HDAC antibody (green) to define the efficiency of silencing and A2B5 antibody (red) as early progenitor marker or O4 (red) to identify differentiating cells.